



Continuous fluid circulation in Hammam Faraun geothermal system, Gulf of Suez rift, Egypt: evidences from hydrothermal deposits along rift-related faults

A. Shawky¹ · M. I. El-Anbaawy¹ · N. A. Shallaly¹ · H. E. Abdelhafiz² · E. N. Shaheen³

Accepted: 5 July 2021 / Published online: 20 July 2021

© The Author(s), under exclusive licence to Springer-Verlag GmbH Germany, part of Springer Nature 2021

Abstract

Geothermal activities are often associated with hydrothermal deposits and hydrothermal features that could aid in geothermal exploration. As a case study, this paper is concerned mainly with the factors controlling the hydrothermal activities and deposits in the Hammam Faraun (HF) area, Gulf of Suez rift, Egypt. In addition to dolomites, hot spring travertine deposits recorded for the first time in this area are emphasized. The proposed conceptual models illustrated that these deposits are confined to the damage zone of the Hammam Faraun fault (HFF). The main factors controlling the hydrothermal activities through time are: syn-rift volcanic activities related to shallow magma chamber bounded to the lithosphere, variable fluid conditions and nature of hydrothermal circulation through HF fault system. At rift initiation, sea water percolated along the CLB fault (a clysmic fault parallel to HFF), reached the Nubian Sandstone and Eocene Carbonate aquifers, mixed with their water, heated and arose along the HFF. The hydrothermal deposits related to fluid circulation at this time are represented by stratabound dolomite. At rift climax, the massive dolostone was formed from coastal lakes mixed water. These dolomitizing lakes occupied the topographically low area at the flank of HF relay ramp. With the beginning of post rifting time, travertine deposits were developed from fluids inside spring lakes during the Pleistocene pluvial period. This sequential development of dolomitization, travertine, and hot fluid flow in HF area would suggest continuity of geothermal activities since the rift initiation until present. Therefore, this study may be considered as a guiding model for further proper evaluation of geothermal energy resources of HF area in particular and geothermal systems in rift basins in general.

Keywords Gulf of Suez rift · Hammam Faraun (HF) · Geothermal fluids · Hydrothermal dolomitization · Travertine · Oligo-Miocene volcanic activity

Introduction

Geothermal activities can be classified according to their relation to plate tectonics, heat sources, heat transfer processes, chemistry of fluids, and fluid pathways (e.g., Moeck 2014). Worldwide occurrences and utilizations of geothermal energy resources are found along or near tectonic plate boundaries and favorable tectonic settings where,

earthquakes, volcanic activities, hot spots, thermal and hydraulic anomalies are concentrated (e.g., Boden 2017). Egypt is located in a tectonic setting that enriches its geothermal potentialities where it is surrounded by three types of present-day plate boundaries, the Hellenic convergent plate boundary in the Mediterranean, the Red Sea divergent plate boundary and the Gulf of Aqaba- Dead Sea plate boundary transform fault (e.g., Morgan and Swanberg 1979; Abdel Zaher et al. 2012 and references therein).

Intracontinental rifts represent one of the favorable tectonic settings for convection-dominated geothermal play systems, these systems are mainly fault-controlled (Moeck 2014). The Gulf of Suez rift comprises several geothermal manifestations e.g., Ayun Musa, Hammam Faraun and Hammam Musa (Fig. 1a).

The hot springs of the Hammam Faraun area (Fig. 1a) which record the highest measured temperature of thermal

✉ A. Shawky
ashawkym@sci.cu.edu.eg

¹ Geology Department, Faculty of Science, Cairo University, Giza, Egypt

² National Research Institute of Astronomy and Geophysics (NRIAG), Helwan, Cairo, Egypt

³ Aminex Petroleum Eqty Ltd, London, UK

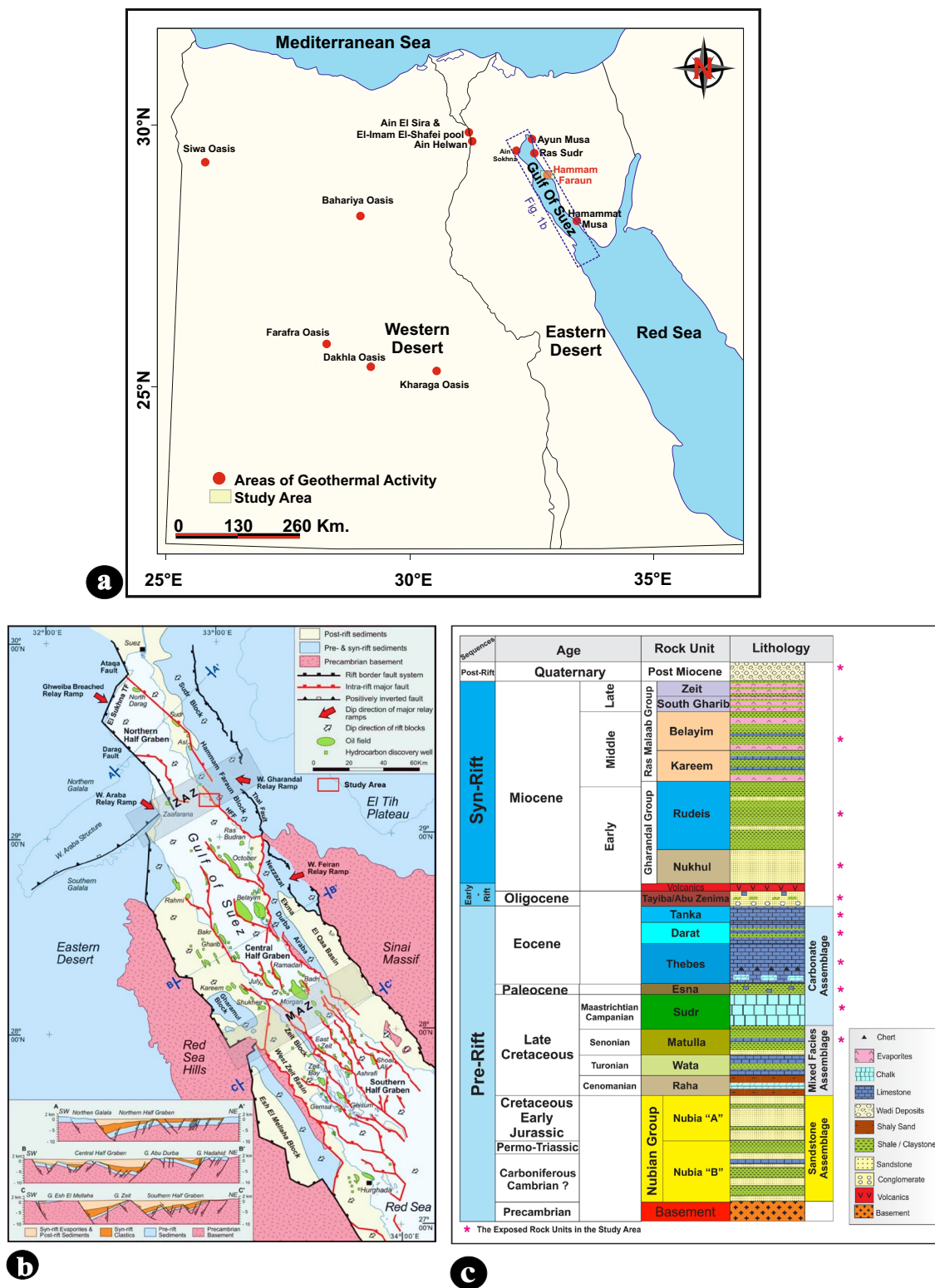


Fig. 1 a Location map of Hammam Faraun area within the geothermal activity map of Egypt (Compiled from different sources). **b** Regional structural map of the Gulf of Suez rift. Hammam Faraun rift block is located within the central dip province and bounded by two

major faults which are HFF and Thal fault (modified after Moustafa and Khalil 2017). **c** Simplified stratigraphic column of Hammam Faraun rift block including the study area (adapted from Moustafa and Abdeen 1992; Sharp et al. 2000)

springs in Egypt (up to 70 °C, e.g., El Ramly 1969; Morgan et al. 1983), is of significant balneotherapeutic and geotouristic values. The area comprises pre-rift to post-rift sedimentary rock units and volcanics as well. Previous geothermal studies (e.g., Boulos 1989; El-Qady et al. 2000; Atya et al. 2010; Abdel Zaher et al. 2011, 2012; Lashin, 2013) were carried out and both conceptual and numerical models for the geothermal energy resources of Hammam Faraun area were constructed based on geological, geochemical, and geophysical data. These models suggested that the heat source of Hammam Faraun geothermal system is high heat flow and deep water circulation controlled by faults associated with the Gulf of Suez rift. The main source of this water is meteoric water with some contribution of sea water. Numerical models showed that the estimated reservoir thickness was about 500 m and reservoir temperature between 95 and 150 °C. The value of the estimated potential for was between 12.4 and 19.8 MW and the estimated reservoir production life was 30–50 years. Therefore, Hammam Faraun geothermal site was recommended by these authors as a promising (or may be the most promising) site for geothermal energy development in Egypt.

The studied hydrothermal fluids show obvious dual selective impact on the sedimentary rocks. This impact is observed as dolomitization near to the hot springs (e.g., Hollis et al. 2017) and some spring deposits (travertine). This study focusses on better understanding the relation between fluid circulation and the hydrothermal deposits recorded in the area. The current research is concerned with the field occurrences, petrographical characterization and geochemical interpretations of the different hydrothermal deposits and their genetic relationship to the geothermal fluid circulation in the Hammam Faraun geothermal system. Moreover, integrated conceptual models are constructed to show the different elements of the geothermal system that assumed to control not only the formation of the recent localized hydrothermal dolomite that was previously studied by some authors (e.g., Magaritz and Issar 1973; Hirani 2014; Hollis et al. 2017; Hirani et al. 2018a, b; Korneva et al. 2018) but also the travertine spring deposits recorded by the authors for the first time in the study area as well as some associated karstic features. It is worth mentioning that the previous hydrothermal studies in the study area are important basis for the new dolomitization models presented in this work. However, modifications are made based on the present analyses and results.

Geological setting

The Gulf of Suez rift is differentiated into three major dip provinces or half grabens dominated by NW–SE trending normal faults. The northern, central, and southern half

grabens are dipping toward SW, NE, and SW directions, respectively (e.g., Moustafa 1976; Patton et al. 1994; Bosworth and McClay, 2001). Each half graben is divided into several rift blocks (Fig. 1b). Hammam Faraun rift block is one of these rift blocks. It is a ca 20 km wide and ca 40 km long fault-bounded, crustal-scale block located in the central dip province of the rift (e.g., Moustafa and Abdeen, 1992; Sharp et al. 2000).

The stratigraphic succession of the eastern side of the Gulf of Suez rift is characterized by three main depositional sequences relative to the rifting event, those are: pre-rift (Cambrian to Eocene) sequence unconformably overlying the Precambrian basement rocks); early and syn-rift (Oligocene—Miocene) sequence and post-rift (Pliocene to Recent) sequence (e.g., Moustafa and Khalil, 2017).

In the HF rift block, the pre-rift sequence (about 2000 m thick) includes from the base to top, a clastic Cambrian to Early Cretaceous Nubian Sandstone, a mixed facies assemblage of Late Cretaceous Raha, Wata, Matulla and Sudr formations and a non-clastic assemblage of Late Cretaceous Sudr Formation and Eocene Thebes, Darat and Tanka formations). The early and syn-rift sequence includes the Oligocene clastics (Tayiba and Abu Zenima formations), early rift basic volcanics and Miocene clastics and evaporites. The post-rift sequence is composed of Pliocene to Recent sediments which are mainly wadi deposits (e.g., Moustafa and Abdeen 1992; Moustafa and Khalil 2017) (Fig. 1c). It is worth mentioning that the study of partially dolomitized, pre-rift, Early Eocene Thebes Formation is one of the chief targets of this study.

Methodology

The present study is based on detailed field investigation that led to the construction of a new geological map for the study area with more precise rock boundaries, mapping new volcanic bodies as well as more detailed structural analysis including the major crustal Hammam Faraun fault (HFF). Landsat 8 and Google Earth[®] satellite imagery were substantiated by detailed field work and previous maps to create the detailed geological map. Petrographic studies were done on fifteen collected samples representing the different rocks with special emphasis on the hydrothermal deposits. Cathodoluminescence (CL) analyses of two selected samples were carried out using a cold cathodoluminescence system, mounted on Nikon eclipse 50 T optical microscope at pressures of < 50 Torr, 10–15 kV and a cathode current of 350–500 μ A. Two selected dolostone samples which were collected from the hot spring site of HF, were prepared for SEM. Field emission scanning electron microscope between (SEM) Hitachi S-4700 equipped with a NORAN vantage energy dispersive spectrometer (EDS). SEM analyzes using

15 mm working distance, 10 kV acceleration voltage, and a semiconductor Si (Li) detector. The samples were mounted on SEM holders with silver glue and coated with C. All these techniques were performed at the laboratories of the Institute of Geological Sciences at Jagiellonian University, Poland. Water quality equipment was used for in situ measurements. The primary field measurements (temperature, pH, and TDS) of the thermal waters of the hot springs were performed using standard calibrated portable equipment. Temperature and pH were measured using ADWA AD130 proof PH-ORP-TEMP portable meter, while TDS was measured using ADWA AD410 standard professional TDS-TEMP portable Meter. Three samples were collected in acid-washed polyethylene bottles and kept refrigerated till transformation to the laboratory. Chemical analyses of the thermal water samples were carried out at the National Water Research Center (NWRC), Egypt. Laboratory analysis included major ions measurements. Major anions were

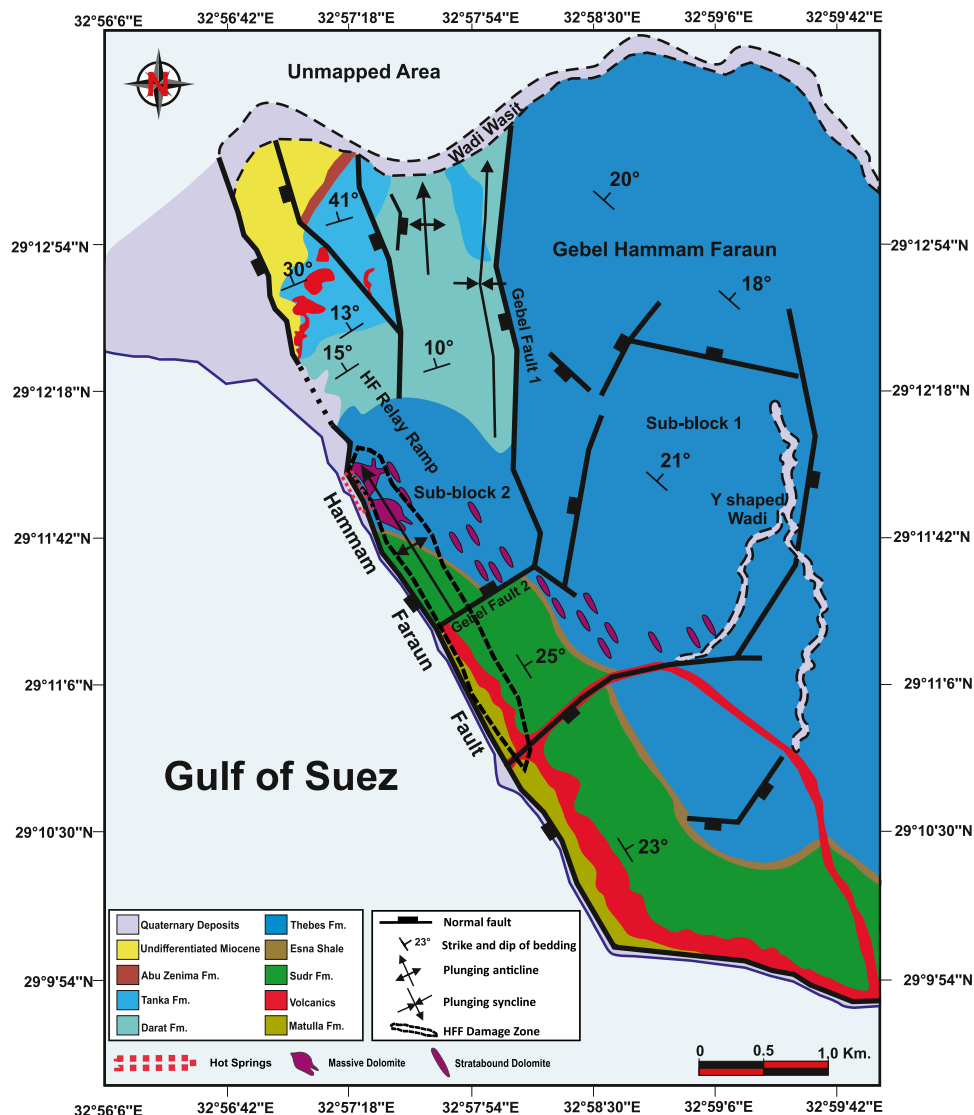
estimated by Ion Chromatography (IC). Major cations were estimated using inductively coupled plasma-optical emission spectrometry (ICP-OES). A representative sample from the three samples is used in this paper.

Results

Structural setup

Structurally, the study area is subdivided by the so-called Gebel fault (GF) into two tilted sub-blocks; a main sub-block (sub-block 1) to the east and southeast and a smaller sub-block (sub-block 2) to the northwest (Fig. 2). The name Gebel fault was given by Hirani (2014). In this study, we refer to the two segments of the Gebel fault to Gebel fault 1 (GF 1) and Gebel fault 2 (GF 2). The main sub-block is delimited westerly by the NNW-oriented GF 1, the ENE

Fig. 2 Geological map of the study area showing the distribution of different rock units, volcanic occurrences, structural elements as well as hydrothermal deposits (after Moustafa 2004 and Hollis et al. 2017 with major modifications)



oriented GF 2, and the NW and WNW-oriented segments of HFF. This sub-block has a nearly constant dip direction toward NE. At the southwestern boundary of this sub-block, the dip changes toward SW direction as a result of the occurrence of a footwall anticline of the HFF. In addition, the dip varies locally within the eastern part of this sub-block due to the occurrence of intra—sub-block faults. The small sub-block (sub-block 2) has variable dip directions that range between NNE to NW with the predominance of the NW dip direction. The variation in dip direction of this block is attributed to two main processes; relay ramp formation and drag folding associated with the GF and HFF.

An overlapping transfer zone is formed between the right-stepped HFF and GF 1, where the throws of the two faults are strongly decreased to zero at their terminations. This transfer zone (Fig. 2) was formed as a relay ramp (monocline) dipping toward NW direction which resulted in the accumulation of the basal Miocene deposits at the north western part of the study area. Most probably, after the deposition of the basal Miocene, the relay ramp was breached and resulted into the formation of the NE-oriented segment GF 2. We referred to this relay ramp as HF relay ramp.

Two types of folds are recorded in the study area. These folds are next to the major faults with their axes orientated

parallel to sub-parallel to the fault strike (Fig. 2). The first type comprises two folds, a NW plunging fold in the footwall of the HFF and a syncline plunging to the north in the hanging wall of the GF1. The second type of folding occurs as NW plunging rollover anticline in the hanging wall of the GF1. The western limb of this anticline is collapsed by mappable and unmappable northwest oriented normal faults.

The large displacement (about 5 km) of the HFF resulted in the formation of a 350–500 m wide damage zone where the hot springs exist (Fig. 2). The inner part of the damage zone is characterized by brecciation, fragmentation and high frequency of fractures and veins which strongly obliterate the original bedding (Fig. 3). The outer part of this damage zone is dissected by extensive fractures; those are NW oriented conjugate fractures and nearly vertical extension fractures. It's noteworthy that the hydrothermal features that will be discussed later are concentrated within the damage zone of HFF.



Fig. 3 Field photos for the damage zone of the Hammam Faraun Fault showing fracturing, brecciation, and Fe oxide staining. **a** Fracturing and nearly vertical slip planes in the outer core of the damage zone. **b** Cavities and open space crystallization in the heavily crushed part of the inner core of the damage zone. **c** Distal view showing the

inner and outer cores of the damage zone. **d** Narrowing of the damage zone in the exposed part of the Sudr Fm. and Esna Shale showing small number of fractures filled by calcite and gypsum and blackening of some shales probably induced by hydrothermal fluids or the depositional condition of shales

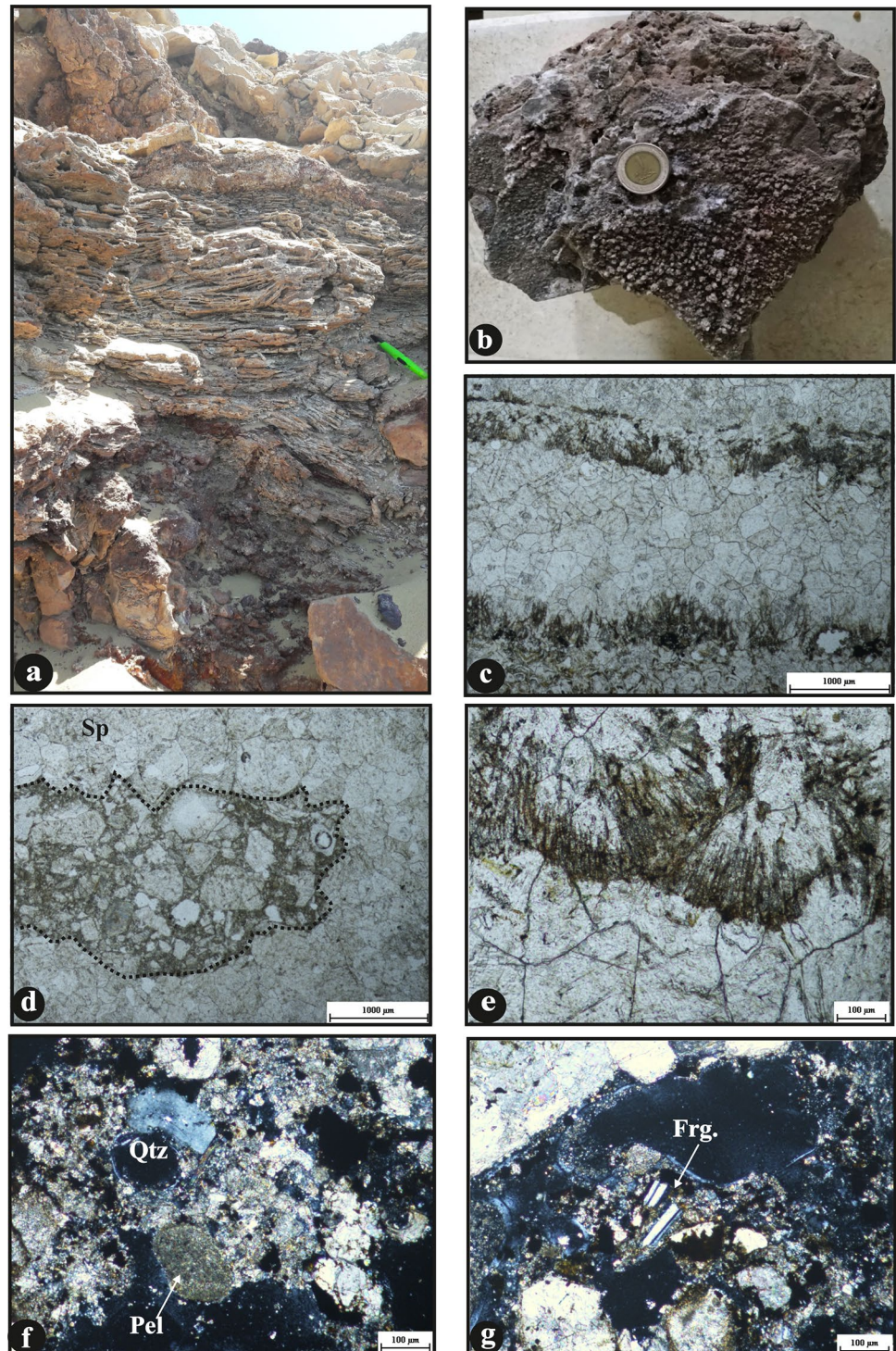
Hydrothermal features and deposits

Travertine

Geomorphologically, travertine deposits are of cascade type as they are formed along the steep slope of the fault scarp of the HFF. They occur in the form of isolated

patches and masses with an estimated area of 1 m² each. These deposits are hosted in the Thebes carbonates, about 250 m south of the HF springs (Fig. 4a). They are restricted in certain horizons along the damage zone of HFF. These deposits consist of nearly horizontal, alternating pale brown and centimeters -thick crenulated bands that strike NW–SE. Cavities in between are variably

Fig. 4 Travertine deposits recorded in the study area. **a** Field photo showing a general view of a laminated travertine mass, note the presence of brecciation and reddish coloration along their contacts with the Thebes limestone. Looking NE. **b** A hand specimen of the travertine showing a few, centimeter- sized gas escaping pores. **c** A thin section showing alternating sparite, micrite, and microbial laminae, PPL. **d** A lens of floated calcitic patches in a micritic matrix, PPL. **e** Fan shaped primarily aragonitic crystals percolating the calcite crystals, PPL. **f** Detrital rounded quartz (Qtz) grain and peloids (pel) in the travertine, CN. **g** A disintegrated glassy basaltic fragment, with plagioclase micro-phenocrysts, set in a cavity, CN



sized, elongated and parallel to the banding. Within these cavities, large calcite crystals grew perpendicularly from the walls to the center. This travertine exhibits gas layers which are composed of rounded to elongated cavities especially at its upper surface (Fig. 4b). The gradational contact with the Thebes carbonates exhibits pronounced brecciation and reddish to blackish coloration (Fig. 4a). The bands were affected by oblique fractures of different orientations.

Petrographically, the travertine is composed of very thin occasionally crenulated flat lamina (Fig. 4c). Two generations of carbonate in this travertine are recorded; an older fine-grained micrite that contain minute crystals and lithic fragments (Fig. 4d) and a younger and dominant sparite crystals with sharp crystal faces constitute about 90% of the rock (Fig. 4c, d). The blocky sparite has scalenohedral shaped terminations and growing perpendicular to the cavity walls which host relict micrite (Fig. 4c). Microbial laminas are also present (Fig. 4c). These features are characteristic for hot water travertine (Flügel 2004; Scholle and Ulmer-Scholle 2003). Clots of fan-shaped primarily aragonitic crystals that sometimes fill the fractures are frequent (Fig. 4e). Minute detrital quartz grains and peloids are occasionally dispersed in the travertine (Fig. 4f). Disintegrated lithic fragments of glassy plagioclase-phyric basalts are sporadically set in the micritic matrix (Fig. 4g).

Karst features

One of the most conspicuous features in the HFF damage zone is the presence of karstic features in the Thebes Formation. These features have either a dissolutional or a depositional nature. Cavities and midget caves are the most common dissolution forms (Fig. 5a). The main HF hydrothermal spring cave represents one of the large exposed midget phreatic caves in the study area (Fig. 5b). This cave has been developed when a part of the Thebes carbonate host rock was highly fractured and jointed and then collapsed from the ceiling of the cave opening as a result of the repeated undercutting erosion. Fluid sources for the karstification process probably include rainwater as well as thermal springs water. Some cavities and fractures are filled with salt crusts or with Terra Rosa and red matrix debris which constitute the depositional karstic features within the hot springs area (Fig. 5c).

Dolomitization

The field investigation of the study area shows partial to complete dolomitization of the Thebes carbonate in the foot-wall of HFF. The majority of the darker dolomitized limestone beds are concentrated near the fault zone within the lower part of the Thebes Formation where they are highly fractured and tilted. On the other hand, the upper part of the



Fig. 5 Karstic features in the Early Eocene Thebes Fm. in Hammam Faraun hot springs area. **a** Cavities and midget caves representing the dissolution features. **b** HF main cave, the largest midget dissolution-

related cave in the study area. **c** Salt crust, Terra Rosa and red matrix debris inside HF main cave

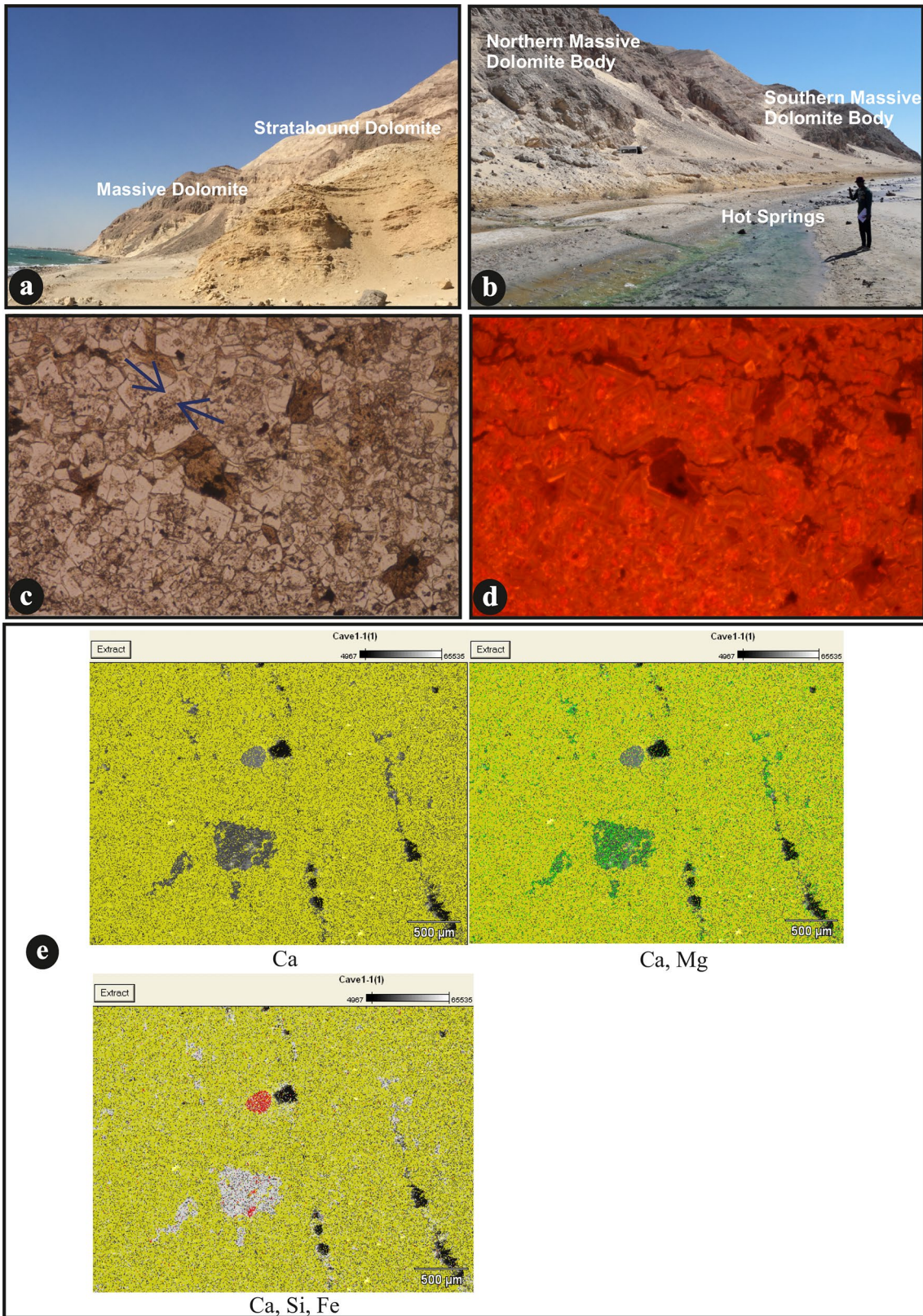


Fig. 6 Dolomitization within the Thebes Fm. in the study area. **a** Field photo showing the two modes of occurrence of dolomite namely; stratabound and massive dolomites previously named by Hollis et al. (2017). **b** The two main massive dolostones bodies located within the HF relay ramp and within the HFF damage zone, nearby the hot springs. **c** Dolomite in plane polarized light (PPL), euhedral to subhedral dolomite rhombs replaced the host Thebes limestone with cloudy centers (high inclusions) and limpid borders. **d** Cathodoluminescence (CL) image of the dolomite in (c). The cores of the rhombs show more luminescence than the borders which show zonation. Some rhombs are completely zoned without any core. **e** SEM/EDS of dolomite sample from the ceiling of the main cave. This can be interpreted as a dolomite crystal Ca (yellow) and Mg (green) enclosing a clay particle having high concentration of Si (white), Al (white), Mg (green) and Fe (red). Another phase of Fe (red) could represent pyrite

Thebes formation consists of chalky laminated fossiliferous limestone showing weathered surface and karstification (Fig. 6a). Additionally, similar dolomitization in the hanging wall was also observed from the subsurface well logs (Shawky 2020).

According to the spatial distribution of these dolomitized rocks, two main mode of occurrences were recorded as stratabound dolostones and massive dolostones. The stratabound dolomitic rocks are dark brown in color occurring as scattered bodies of variable dimensions and are parallel to the bedding of the Thebes Formation. These bodies are more numerous and frequent close to HFF and vanishes away from the hot springs. They are commonly associated with scattered flint nodules. The other type of dolomite bodies; the massive ones are more reddish in color. There are at least two major massive dolomitic masses of nearly similar dimensions, each with average thickness of 100 m and width from 300 to 500 m, one exist to the north of the study area and the other to the south (Fig. 6b). They are located within the HF relay ramp and within the HFF damage zone, nearby the hot springs (Fig. 2). They are structurally confined by the major steeply sub-vertical NNE-SSW to ENE-WSW trending fractures. The fracture swarms of the outer part of the HFF damage zone represents the outer boundary of the massive dolostone bodies where unaltered limestone appear gradationally to the east. These two bodies exhibit fracturation and irregular brecciation. The HF caves exist within the northern massive dolostone body and the travertine deposits are about 250 m away.

Under petrographic microscope, euhedral to subhedral dolomite with zoning crystals is commonly observed (Fig. 6c). Scattered dolomite rhombs are randomly distributed through the pore spaces. Some of these rhombs are distributed along stylolites and pressure dissolution seams as well as late cavity-filling (Fig. 6c).

Thin sections show the rhombic structure of the dolomite though no obvious zoning. On the other hand, the cathodoluminescence (CL) microscopy shows a pronounced zoning

within each rhomb (Fig. 6d). There is an alternation of bright and dull luminescence. Some dull-luminescent dolomite crystals are cored with bright- luminescent dolomite (bright red and orange), others are cored by bright-luminescent calcite (yellowish colored), though some rhombs have no older cores and are composed mainly of recently formed dolomite (Fig. 6d). The CL images preserve the carbonate residues in between the dolomite in the form of non-luminescent areas (Fig. 6d). SEM/EDS analysis of selected sample from the ceiling of the main cave within the hot springs area are presented (Fig. 6e). It is obvious that the rock is heterogeneous and is composed mainly of dolomite with Ca (yellow) and Mg (green) except in areas which occupied by other minerals (Fig. 6e). C is not detected as it is from the light elements that cannot be detected by the EDS technique as reported earlier (Severin 2004). Clay particles are also detected in the EDS images having high concentration of Si (white), Al (white), Mg (green) and Fe (red). This clay particles may be montmorillonite as inferred from the elemental concentration. Another minute phase is detected which is composed mainly of Fe (red), this could be pyrite (Fig. 6e).

Volcanic activities

The volcanics are exposed in the northern part of HF area in the form of sills that intrude the Tanka Formation, and flows underlying Miocene clastic (Fig. 7a). In the SE part, they are represented by a sill-dyke complex within the Matulla-Thebes formations (Fig. 7b, c). These Tertiary volcanics are mainly doleritic and amygdaloidal basalts showing fracturing and high alteration. The sills and dykes enclose differently sized xenoliths of the sedimentary rocks on which visible thermal effects of the basalts are observed. It is worth mentioning that the doleritic sills intrude the Wata and Sudr formations are recorded in the hanging wall of HFF (Shawky 2020).

Petrographically, the interior of the sills is holocrystalline olivine dolerite that is characterized by intergranular texture with variable amounts of plagioclase and augite (Fig. 7d). Whereas the lava flows, dykes, and the margins of the sills the rock is holocrystalline to cryptocrystalline plagioclase-phyric basalts. The glassy mesostasis of the cryptocrystalline variety exhibits different degrees of devitrification. The Plagioclase (mainly labradorite) forms phenocrysts and micro- phenocrysts as well as microlites in the matrix (Fig. 7e). Pyroxene (mainly augite) and olivine which is commonly altered to iddingsite, form micro- phenocrysts. Both plagioclase and augite form doleritic texture and flow texture within the doleritic and olivine basaltic varieties, respectively. Patches of sericite, smectite (montmorillonite) and calcite are dispersed in the glassy mesostasis due to the effect of the glass alteration. Calcitization of the glassy mesostasis of these volcanics suggests the presence of CO₂-rich

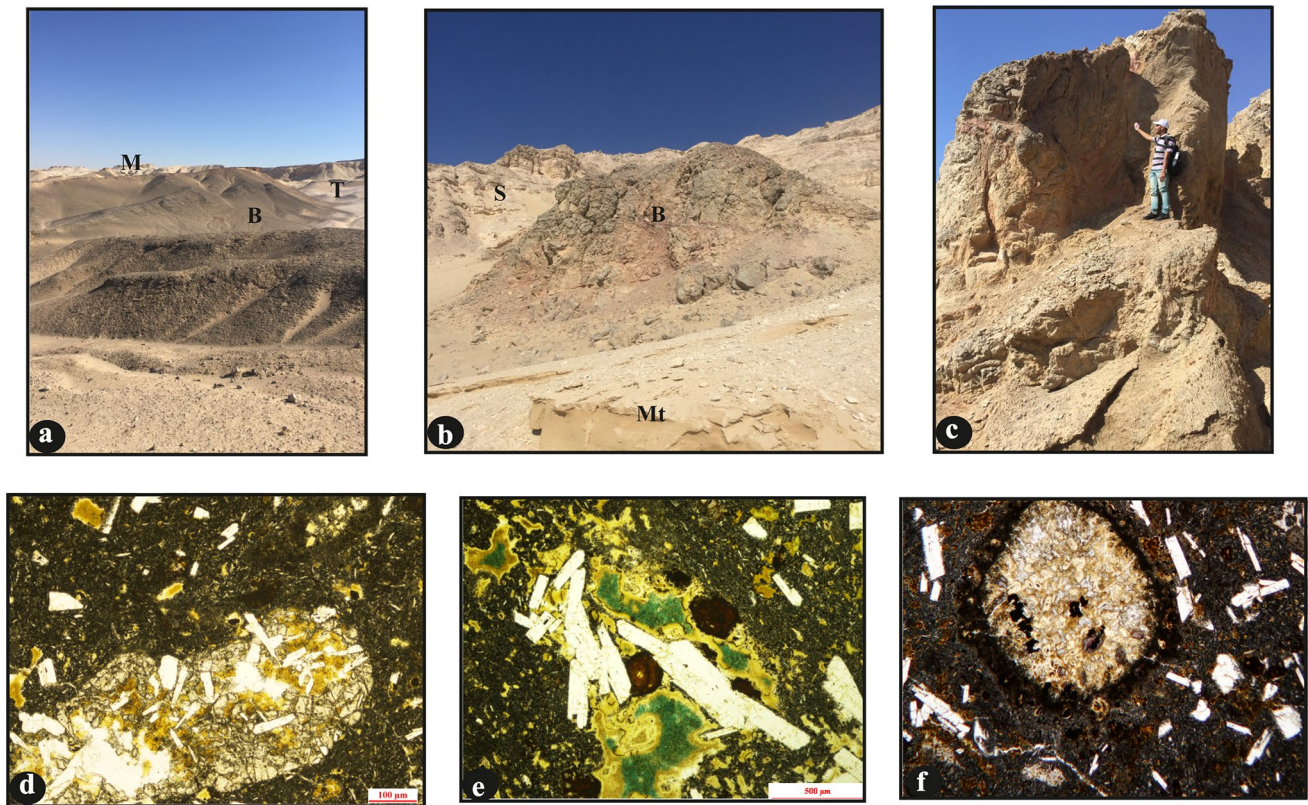


Fig. 7 Oligo-Miocene volcanic occurrences in the study area. **a** A General view of the NW part of HF area showing the basaltic flows (B) overlain by the Miocene clastics (M) and underlain by Tanka Formation (T), looking NW. **b** A doleritic sill (B) intrudes the Sudr chalk (S) and Matulla Fm. (Mt), SE of Hammam Faraun area, looking N. **c** A spheroidally weathered basaltic dyke, note the presence of reddish alteration of the Sudr Formation at the uppermost part as a result of high temperatures fluids. Looking NW. **d** An olivine dolerite enclave

in the hypocrySTALLINE plagioclase-augite-phyric basalt. PPL. **e** Prismatic subhedral plagioclase microphenocrysts imbedded in the glassy mesostasis, plagioclase-phyric basalt, note the presence of zoned amygdules with green celadonite followed rim-ward by yellowish smectite. PPL. **f** A large rounded and resorbed carbonate xenolith in the plagioclase-phyric basalt, witnessing the interaction between the lavas and sedimentary rocks in the area. PPL

fluids during the alteration process. Xenoliths of olivine dolerite and pyroxene-phyric basalt as well as other country rocks such as carbonate (Fig. 7f) are recorded in the basaltic flows. These basaltic rocks are amygdaloidal. The amygdules are numerous, small, elongated to rounded, and exhibit a zonal arrangement of various minerals in different parts of the study area; chalcedony, smectite, then calcite as in the NW part; iron oxide, smectite, then celadonite (Fig. 7e). The alteration product of these volcanics in addition to the minerals fill the amygdules and fractures reflect the effect of country rock composition as well as hydrothermal fluids on these volcanics.

Hydrochemical analysis

The analysis of the chemical composition of the thermal water samples from the study area (Table 1) demonstrates

Table 1 Field data (T, pH and TDS) and chemical composition (major cations and anions; concentrations are in mg/l) of the thermal springs in Hammam Faraun area

Sample	HF-1	HF-2	HF-3	HF-4
T (°C)	70	–	70	70
pH	6.76	–	7.44	6.48
TDS (mg/l)	17,712	14,869	14,030	16,800
Na	4218	3700	3642	4750
K	65	52.78	127	130
Ca	876	1180	966	1039
Mg	189	285	270	489
Cl	6435	8228	8050	9654
SO ₄	2057	690	780	1450
HCO ₃	346	171	109	132
Source	This study	Issar et al. (1971)	Sturchio et al. (1996)	El-Fiky (2009)

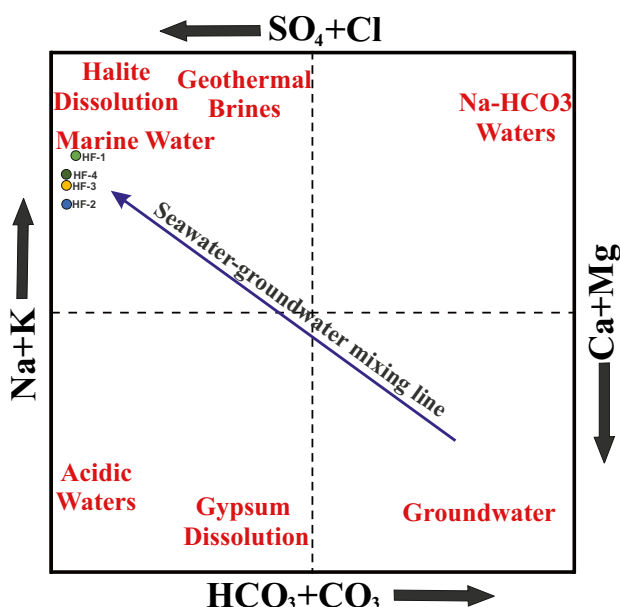


Fig. 8 Langelier-Ludwig diagram (Langelier and Ludwig 1942) for the investigated thermal samples based on the concentrations of major ions. Samples sources: HF-1: this study, HF-2: Issar et al. (1971), HF-3: Sturchio et al. (1996), HF-4: El-Fiky (2009)

that the water is near neutral (pH ~ 6.8), has a salinity of 17,712 mg/l that is much higher than that of a fresh water and far below that of marine water. It is enriched in Cl, SO₄ as well as Na and Ca. The hydrochemical formula (Kurlov formula; Kurlov, 1928) for the present water sample is represented in (Eq. 1). Accordingly, this water is of Ca- Sodium Chloride type.

$$M_{17.71} \frac{Cl_{78.91} SO_{418.62} HCO_{32.47}}{Na_{75.10} Ca_{17.88} Mg_{6.35} K_{0.67}} T_{70} pH_{6.76} \tag{1}$$

Equation 1: Hydrochemical formula (Kurlov formula) for HF-1 thermal water sample (this study). Ions' concentrations are in e% and total mineralization (M) is in g/l.

The main components of HF spring water from current analysis and from previous work are plotted on Langelier-Ludwig diagram (Langelier and Ludwig 1942) (Fig. 8) to reveal their origin. Moreover, several variation diagrams are constructed to illustrate the relation between different ions and chloride, where the seawater dilution line (SWDL) is presented on the diagrams (Fig. 9).

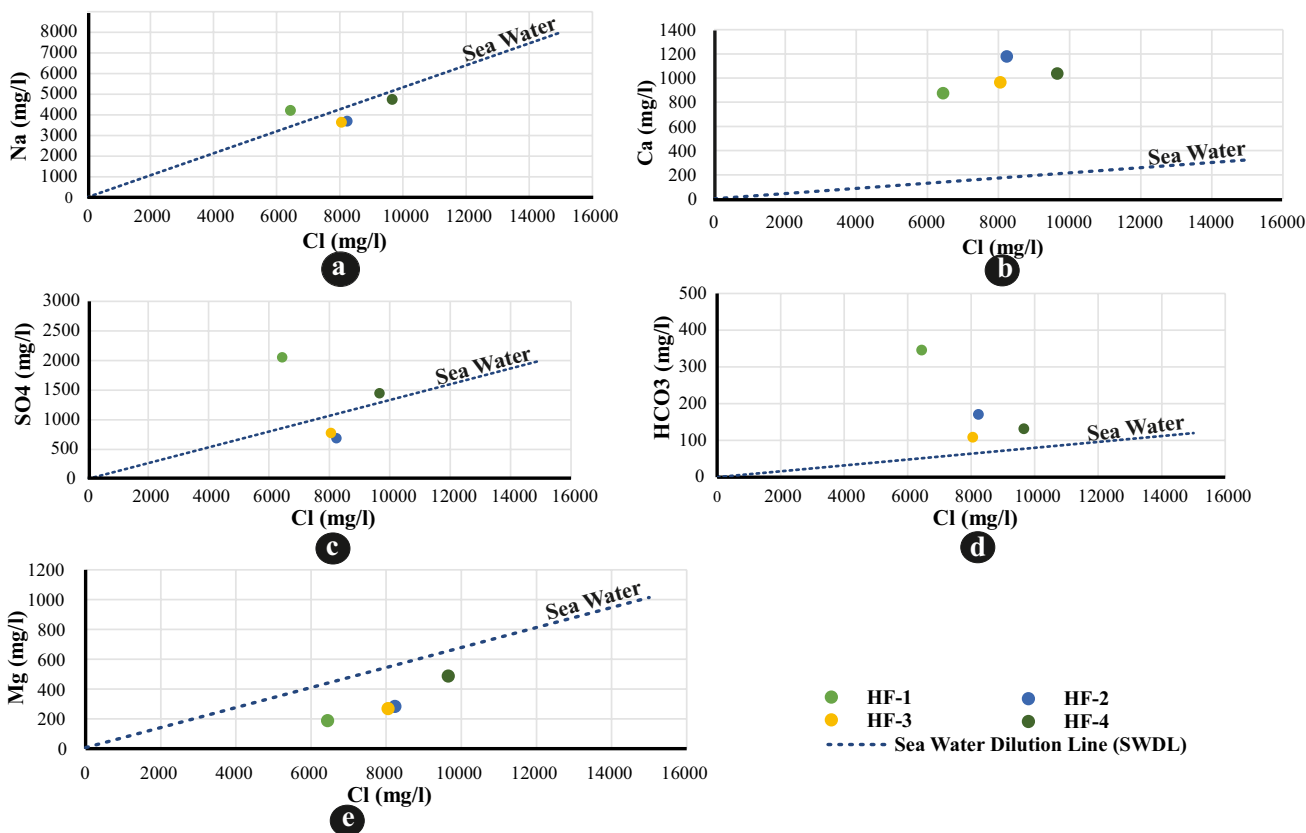


Fig. 9 Chloride variation diagrams illustrating the relation between different cations and anions versus chloride for the investigated thermal water samples. **a** Na against Cl. **b** Ca against Cl. **c** SO₄ against

Cl. **d** HCO₃ against Cl. **e** Mg against Cl. Samples sources: HF-1: this study, HF-2: Issar et al. (1971), HF-3: Sturchio et al. (1996), HF-4: El-Fiky (2009)

Discussion

Hydrochemical origin

The results of the chemical analysis of the thermal water samples in the present study are in some correspondence with those of Issar et al. (1971), Sturchio et al. (1996), El-Fiky (2009) and Abdel Zaher et al. (2011).

Falling of the water samples near the marine water field in the Langelier-Ludwig diagram (Fig. 8) reflects the possible effects of Miocene evaporite dissolution as well as probable mixing with sea water. The relation between Na and Cl indicates that Na concentration in sample HF-1 plot above the SWDL and below the line in the rest of samples, indicating possible cation exchange with the rock matrix (Fig. 9a). The relation between Ca and Cl (Fig. 9b) shows high Ca relative to Cl than in seawater which may indicate calcite and gypsum dissolution of the Eocene Carbonate rocks and the Miocene Evaporites, respectively. The increase of SO_4 and HCO_3 against Cl also indicates gypsum and carbonate dissolution (Figs. 9c, 9d respectively). An important relation is that between Cl and Mg (Fig. 9e) where the decreasing in Mg in all samples is mainly related to the dolomitization process.

The plotting of some samples more or less near to the seawater dilution line in the Cl variation diagrams supports the mixed-water origin assumption. Isotopic studies (Issar et al. 1971) also suggests the mixing of meteoric waters with sea water in both the Nubian Sandstone and the Eocene Carbonates.

Dolomitization models

The origin of dolomite causes much debate and difficulties, particularly in the case of pervasive dolomitization of extensive limestone as in HF rift block. The major problems in the dolomitization process are the source of dolomitizing fluid with its Mg content and the mechanism of fluid circulation and penetration through the carbonate host rocks. In trying to unravel these problems, several models for dolomitization were discussed by many authors, such as Tucker and Wright (1990), Tucker (1991), and Warren (2000). However, the most recent studies which have been applied to the study area, are those of Magaritz and Issar (1973), Hollis et al. (2017), and Hirani et al. (2018a, b).

The stratabound dolomitization model

Based on the results of this study and the subsurface data of Shawky (2020), we mostly agree with Hollis et al. (2017) and Hirani et al. (2018a) concerning the proposed model of

the formation of stratabound dolomite. They proposed that the fluid circulation took place along faults related to progressive rifting, being heated within the Nubian Sandstone. In this work, we proposed the circulation of fluids between HFF and CLB fault (a clysmic fault in the hanging wall of the HFF; Shawky 2020). The fluids were heated within both the Thebes and Nubian geothermal reservoirs. This is evidenced by petrophysical analysis of these geothermal reservoirs in some offshore wells (Shawky 2020). Previous studies assigned the high heat flow associated with crustal thinning that accompanied the rifting process and the radiogenic heat produced from basement rocks underneath HF area as sole source of heating (e.g., Morgan et al. 1985; El-Qady et al. 2000; Abdel Zaher et al. 2012). However, an important heat source which has not received adequate attention is the presence of basaltic magma storages at a depth of about 15–20 and 25–30 km bounded at the base of the lithosphere as reported by Shallaly et al. (2013). It is possible that sea water along with modification, could be the dolomitizing fluid (Tucker 1991). Based on the results of $^{87}\text{Sr}/^{86}\text{Sr}$ and REE signature of the HF dolomites, Hollis et al. (2017) and (Hirani et al. 2018a) concluded that the Oligo-Miocene sea water was the only available fluid within the observed temperature range, with sufficient volume and Mg/Ca ratio for the stratabound dolomitization with a possible contribution from entrained seawater in Nubian Sandstone which may also have contributed to circulation. However, current research proposes that the dolomitizing fluid that was available for stratabound dolomite formation is a mixed fluid consisting of modified seawater and formational fresh to brackish water of both Nubian Sandstone and Thebes Formation that underwent circulation along faults within HF geothermal system.

The massive dolomitization model

The present study confirms the localization of the formation of the hydrothermal epigenetic massive dolomite within the damage zone of the HFF inside a relay ramp near the present day hot spring area as “fracture Corridors” bounding the massive dolostones bodies probably played a part in barring the lateral flux of fluids away from HFF damage zone, this is supported by the nonexistence of massive dolostones elsewhere on the HFF block (Rotevatn and Bastesen 2014; Hollis et al. 2017 and Hirani et al. 2018a, b). However, in this study, a model for the evolution of the HF rely ramp is presented (Fig. 10). At Early Miocene times, the transfer zone between the HFF and GF1 was established in the form of NW-dipping monocline (HF rely ramp). This was breached later to produce the NE-oriented GF2 (Fig. 10). Accordingly, the localization of the hydrothermal fluids was controlled by the topographic low area at the toe of HF relay

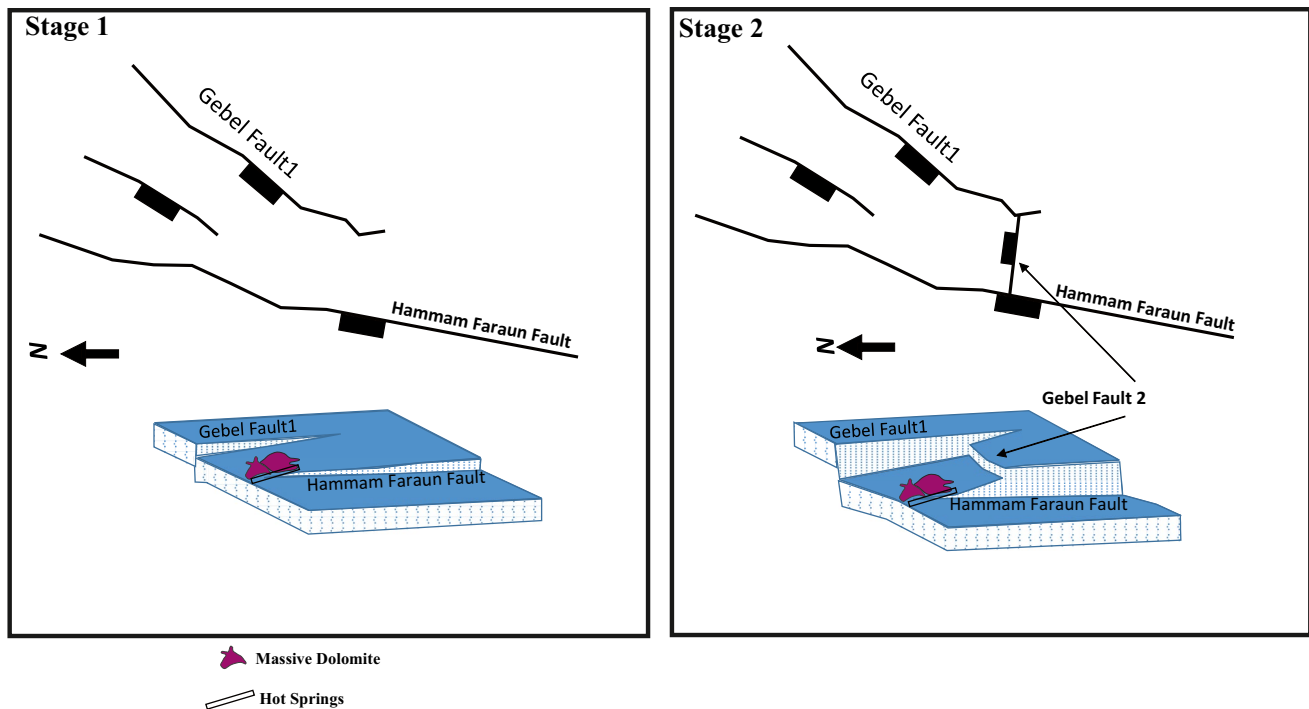


Fig. 10 Schematic evolutionary model of Hammam Faraun relay ramp enclosing the massive dolostones bodies. Stage 1: Formation of a relay ramp (monocline) between the right-stepped overlapped HFF

ramp and resulted in the formation of lakes where dolomite was formed.

Therefore, our proposed model could represent a “mixed coastal lake model” similar to the model proposed by De Deckker and Last (1988) for the modern dolomite deposition in continental saline lakes at Victoria, Australia. These massive dolomites could have been formed by mixing of modified sea water flux and ancient Mg-rich brines similar to that proposed by Mehmood et al. (2018). These hot brines probably have come into contact with fresh continental meteoric or drainage water discharging into coastal lagoonal depressions or lakes under evaporitic environments (Fig. 11). In this situation, salinities were decreased but Mg/Ca ratios were maintained. The mixing of meteoric groundwater with up to 30% sea water would result in undersaturation with respect to calcite but an increasing saturation for dolomite (Tucker 1991). In the case of seawater recharging, dolomite does precipitate directly from saline lake water where Mg/Ca ratios are high from the interaction of drainage water with weathered exposures of adjacent basalts. However, the multiple phases of dolomitization can be attributed to wide ranging in fluid composition and/or fluid temperatures. Fluid temperatures could have varied as a result of footwall uplift, whereas fluid composition might have evolved through time by fluid-rock interaction or by changes in seawater chemistry (Hirani et al. 2018a, b). This environment is supported by

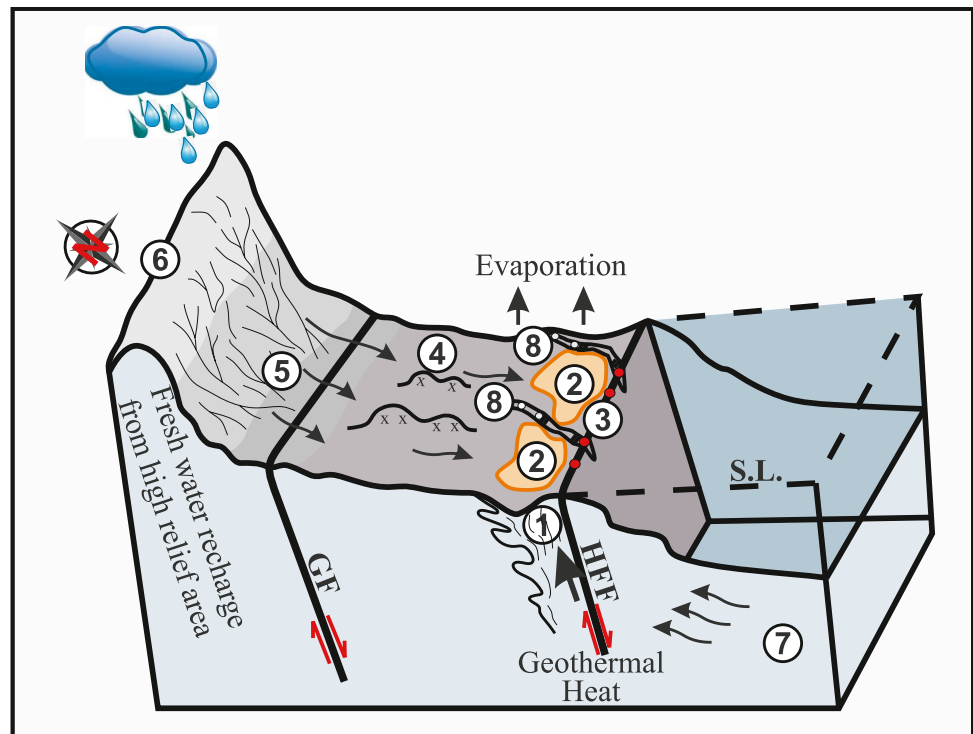
and Gebel fault 1. Stage 2: Breaching of the relay ramp and formation of the NE-oriented Gebel fault 2

the association of smectite and celadonite in the form of olivine alteration or amygdule filling in the adjacent volcanic rocks. This mineral association precipitated from hydrothermally modified sea- or pore-water as reported by Weiszburg et al. (2004 and references therein).

Travertine deposition

Travertines are calcareous, continental deposits exhibiting a very restricted lateral extent, which are mainly deposited from carbonate-rich waters issuing from hot springs. The mechanism of travertine deposition can be explained in the degassing of calcium bicarbonate rich water flowing from hot springs making the water supersaturated in CaCO_3 and so carbonates are precipitated in the form of travertine. Such degassing of carbonate-rich waters is induced by several factors including the drop-in fluid pressure, turbulence of fluid flow, bacterial and algal biological activity extracting the CO_2 from the waters. The environment in which the water flows depends the interaction between these factors which in turn is reflected in travertine morphologies and petrographical characteristics (Chafetz and Folk 1984; Wohletz and Heiken 1992; Ford and Pedley 1996; Guo and Riding 1998; Pentecost 2003; Brogi and Capezzuoli 2009). Many travertines are found to be related to normal fault systems and their associated damage zones. Such structures allow

Fig. 11 Schematic diagram showing a conceptual model of the HF geothermal system during the formation of massive dolomite “mixed coastal lakes model” and later formation of travertine deposits in ponds that existed along the gullies cutting HF fault scarp



①	Damage zone of HFF	⑤	Fresh water runoff
②	Shallow coastal lakes including the massive dolomite sites within the relay ramp zone	⑥	Eocene carbonate outcrops
③	Hot springs (the present day location)	⑦	Sea water intrusion
④	Nearby weathered basaltic exposures with high Mg/Ca ratio	⑧	Gullies within HFF scarp in which travertine is deposited in pools
●	Active Hot Springs	○	Abandoned Hot Springs
■	Travertine	(S.L.)	Sea level
		(HFF)	Hammam Faraun Fault
		(GF)	Gebel Fault

the upwelling, circulation, and channeling of hydrothermal fluids (e.g., Kerrich 1986; Caine et al. 1996; Bellani et al. 2004). Current research revealed that the evolution of the HF travertine resembles that of Terme S. Giovanni travertine fissure-ridge in Italy as proposed by Brogi and Capezzuoli (2009). The HF travertine deposits have been developed from a lime charged underground hot water that issued through nearly vertical fissure along the HFF as spring discharge. Spill of the discharged water was accumulated as restricted local (occasionally hanged) pools around which the vegetation was developed. As wet climate continued, the water table rose in the spring pools and the travertine was deposited under evaporation condition. These pools have existed along the gullies cutting the HF fault scarp and within its damage zone (Fig. 11). The highly fractured damage zone of HFF seems to have guaranteed the circulation and channeling of the hydrothermal fluids that formed the recorded travertine deposits in the area. Abandoned hot springs are suggested to be located around the present location of travertine occurrences from which the hot water flowed near to the

surface along such gullies and deposited travertine. In this way, the present day locations of travertine deposits in the area represent an analog for the past geothermal manifestations. Magnesium is sometimes reported within travertines pointing to derivation from dolomite or mafic rocks nearby the travertine (e.g., Kitano 1963; O’Neil and Barnes 1971; Caboi et al. 1991; Folk 1994). If we interpret the dolomite crystals found in HF travertine as recrystallization crystals, the preexisting dolomites could have provided a source for magnesium. On the other hand, studying the alteration profile along basalt rocks (data reported by Shawky 2020) to measure its contribution in the travertine (if any) was taken into consideration. Comparison of major and trace element composition of the altered and fresh basaltic rocks adjacent to travertine shows dual effect of the alteration on the different elements. Both MgO and CaO decreased from 5 to 0.8 wt% and 10 to 4 wt%, respectively, this is accompanied by enrichment in alumina (14 to 18 wt %). This suggests that the Mg and Ca might be exploited in the formation of travertine. This was supported by the presence of disintegrated

basaltic fragments within the travertine (Fig. 4g). Furthermore, the presence of various sized debris of local derivation inside HF travertine may indicate episodes of torrential steam flow at the peaks of the rainy seasons during the Pleistocene pluvial period. The presence of new generation of calcite spars containing relics of dolomite crystals which may have been formed during dolomitization process of the massive dolostone adjacent to the travertine mounds, may indicate heavily rainfall during Pleistocene pluvial period. Where the temperature of geothermal reservoir is not very high, at less than about 150 °C, travertine is typically deposited (e.g., Boden, 2017). Such reservoir temperatures are characteristic of HF geothermal system (e.g., Morgan et al. 1983; Abdel Zaher et al. 2012; Lashin 2013). Commonly, travertine depositions around hot springs are indicators of geothermal reservoir that may be insufficient to generate electricity as for their not relatively high temperatures but may be utilized for direct-use geothermal applications such as for greenhouses or geothermal heating for nearby districts (e.g., Wohletz and Heiken 1992).

Karstification

The development of the karstic features including dissolution and depositional Karstic forms, depends on regional karst hydrogeological cyclic condition and local geological factors (e.g., lithological and structural variations). The hydrogeological cycles include paleoclimatic fluctuation, particularly rainy and evaporation periodical conditions. All these factors are integrated together to control the development of the Hammam Faraun Karstic features including the hydrothermal spring caves.

Integrated evolutionary model of the hydrothermal deposits

Based on the results of the present study and the previous work, we proposed a model for the evolution of HF geothermal system and the associated hydrothermal features, three stages were predicted. Those are early rifting, rift climax and post-rift climax stages (Fig. 12).

Stage 1: Early stage of rifting (Late Oligocene—Early Miocene)

Mild tectonic activity with slight block rotation took place during this stage. This was accompanied by the emplacement of dolerite dikes and sills driven by high pressure and high temperature of magma intruded the pre-rift rocks.

Hydrothermal activities resulted in the formation of stratabound dolomites especially around the dike-sill complex which acted as an important heat source. At this stage, narrow damage zone of HFF was formed and HF relay ramp began to form but with a gentle dip.

Stage 2: Rift climax (Late Miocene)

During this stage, strong extension, high degree of fault-block rotation and strong fault activity led to a high degree of transmissibility along the fault system which played a leading role in channeling the rising up of the thermal fluids. It was also accompanied by slight volcanic activity in the form of lava flows along the NW part of the area. The damage zone of HFF was widened, relay ramp evolution continued with an increased dip till its final breaching (Figs. 10, 12).

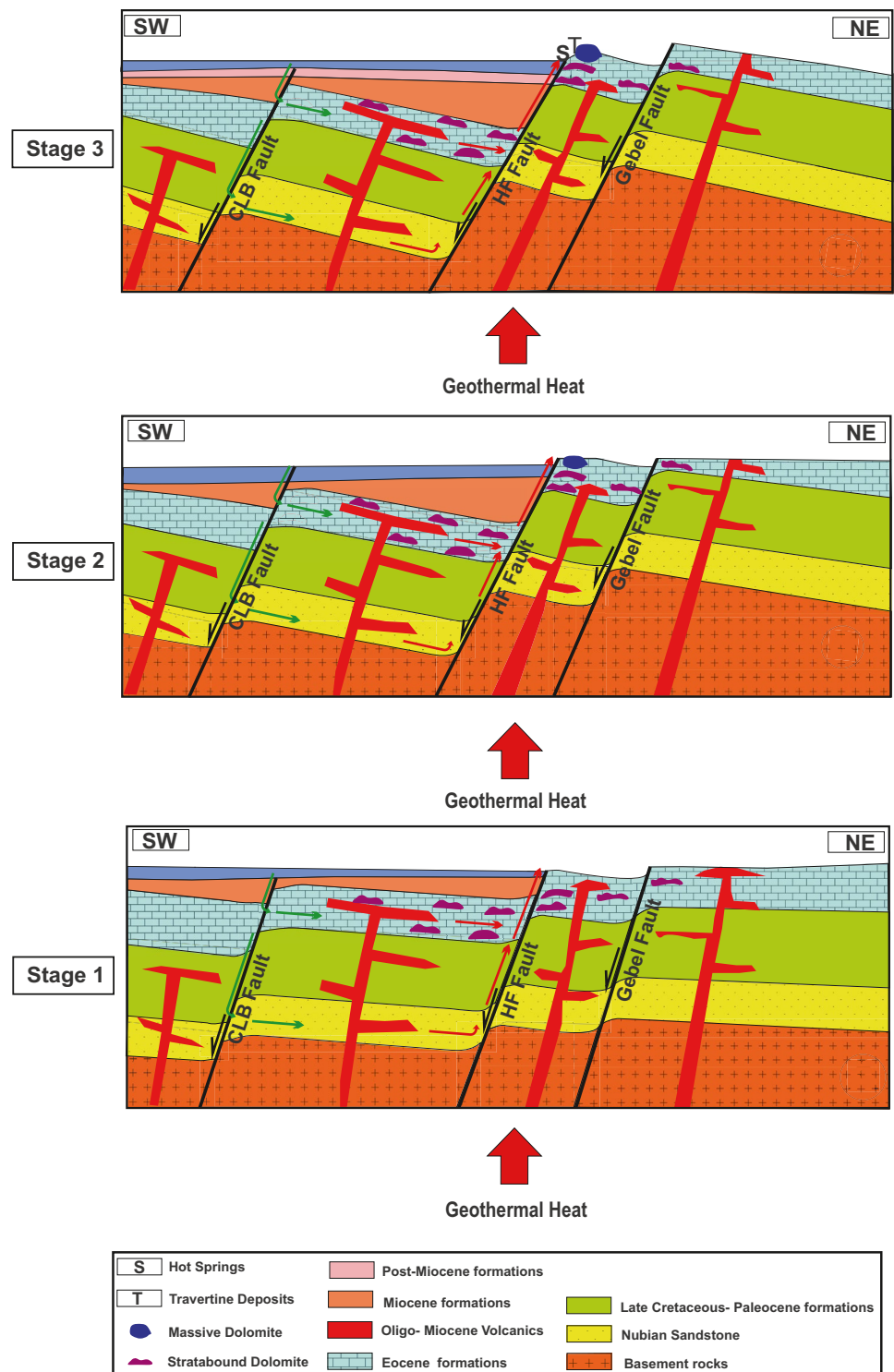
Stage 3: Post- rift climax to present day

The HF relay ramp which was active during the syn-rift period made the area nearby the hot springs a topographically low area in which fluids were concentrated and resulted into the formation of the massive dolostones (Figs. 11, 12). During this stage, tectonic activities slowed down, and the circulation of the hot fluids became driven by dilation of predominant NE and NW oriented fractures within HFF damage zone. Travertine deposits were formed at the expanse of the Thebes carbonate in addition to the alteration of the adjacent volcanic rocks a result of surface flow of hot waters along the gullies, ponds and steps within the HF fault scarp.

Conclusions

In conclusion, the stratabound dolomite, massive dolomite and hot springs travertine have been developed in the HF area at rift initiation, last stage of rift climax and post-rift periods, respectively indicating continuity of hydrothermal activities since late Oligocene till the present. Throughout these different stages, sea water descended along the CLB fault in reaching the Nubia and carbonate aquifers and mixed with their formational water then heated and ascended along the HFF. Heating of these fluids is mainly attributed to the elevated thermal gradient due to the presence of basaltic magma storage at a depth of around 25 km at the base of the lithosphere. The proposed conceptual models of dolomitization and travertine deposition may contribute to proper evaluation of the geothermal resources' potentiality of Hammam Faraun area.

Fig. 12 Schematic diagram showing a conceptual evolutionary model of HF geothermal system and different rift stages accompanied by different hydrothermal deposits. Stage 1: Early rifting marked by stratabound dolomitization. Stage 2: Rift climax the formation of massive dolomite (probably at the last part of this stage). Stage 3: Post Rift climax distinguished by the formation of hot springs (travertine) deposits



Acknowledgements This work is a part of a master’s thesis of the first author registered at faculty of science, Cairo University. The authors are sincerely grateful to Prof. Shawky Sakran (Professor of Structural Geology at Cairo University) for his guidance and valuable discussion during all the phases of this work. Special thanks are given to the staff of the institute of geological sciences at Jagiellonian University in Poland for all their help during the Erasmus+ mobility scholarship

of the first author at their institute where a large part of this work was performed. Prof. Mohamed Hamadan (Professor of Geoarchaeology and Quaternary Geology at Cairo University) is also greatly acknowledged for his constructive discussion on travertine. The authors thank the helpful discussion with Dr. Hend Abu Salem (Lecturer of Hydrogeology at Cairo University) that enhanced the hydrochemical

interpretation. The support from the Egyptian Armed Forces during field trips is highly acknowledged and appreciated.

Funding The field work was financially supported by Cairo University.

References

- Abdel Zaher MA, Ehara S, El-Qady G (2011) Conceptual model and numerical simulation of the hydrothermal system in Hammam Faraun hot spring, Sinai Peninsula. *Egypt Arab J Geosci* 4(1–2):161–170
- Abdel Zaher MA, Saibi H, Nishijima J, Fujimitsu Y, Mesbah H, Ehara S (2012) Exploration and assessment of the geothermal resources in the Hammam Faraun hot spring, Sinai Peninsula. *Egypt J Asian Earth Sci* 45:256–267
- Atya MA, Khachay OA, Abdel Latif A, Khachay OY, El-Qady GM, Taha AI (2010) Geophysical contribution to evaluate the hydrothermal potentiality in Egypt: case study: Hammam Faraun and Swiera, Sinai. *Egypt Earth Sci Res J* 14(1):44–62
- Bellani S, Brogi A, Lazzarotto A, Liotta D, Ranalli G (2004) Heat flow, deep temperatures and extensional structures in the Larderello geothermal field (Italy): constraints on geothermal fluid flow. *J Volcanol Geotherm Res* 132:15–29
- Boden DR (2017) *Geologic fundamentals of geothermal energy*. CRC Press, p 425
- Bosworth W, McClay K (2001) Structural and stratigraphic evolution of the Gulf of Suez rift, Egypt: a synthesis. In: Ziegler PA, Cavazza W, Roberston AHF, Crasquin-Soleau S (eds) *Peri-Tethys Memoir 6: Peri-Tethyan rift/wrench basins and passive margins*. Mémoires du Muséum National d’Histoire Naturelle de Paris, pp 567–606
- Boulos F (1989) Geothermal development of Hammam Faraun hot spring, Sinai-Egypt. In *International conference on applications of solar and renewable energy*, 12 p
- Brogi A, Capezzuoli E (2009) Travertine deposition and faulting: the fault-related travertine fissure ridge at Terme S. Giovanni, Rapolano Terme (Italy). *Int J Earth Sci (geol Rundsch)* 98:931–947
- Caboi R, Cidu R, Fanfani L, Zuddas P, Zuddas PP (1991) Geochemistry of the fountana maore travertines (Central Sardinia, Italy). *Miner Petrog Acta* 34:77–93
- Caine JS, Evans IP, Forster CB (1996) Fault zone architecture and permeability structure. *Geology* 24:1025–1028
- Chafetz HS, Folk RL (1984) Travertines: depositional morphology and the bacterially constructed constituents. *J Sediment Petrol* 54:289–316
- De Deckker P, Last WM (1988) Modern dolomite deposition in continental, saline lakes, western Victoria. *Austr Geol* 16(1):29–32
- El Ramly MF (1969) Recent review of investigations on the thermal and mineral springs. *UAR XXIII Int Geol Cong* 19:201–213
- El-Fiky AA (2009) Hydrogeochemistry and geothermometry of thermal groundwater from the Gulf of Suez Region. *Egypt JKAU Earth Sci* 20(2):71–96
- El-Qady GM, Ushijima K, Ahmad ES (2000) Delineation of a geothermal reservoir by 2D inversion of resistivity data at Hamam Faraun Area, Sinai, Egypt. In: *Proceedings of World Geothermal Congress, Kyushu-Tohoku, Japan* pp 1103–1108
- Flügel E (2004) *Microfacies of carbonate rocks*. Springer, p 976
- Folk RL (1994) Interaction between bacteria, nannobacteria, and mineral precipitation in hot springs of central Italy. *Géogr Phys Quat* 48:233–246
- Ford TD, Pedley HM (1996) A review of tufa and travertine deposits of the world. *Earth Sci Rev* 41:117–175
- Gawthorpe RL, Jackson CAL, Young MJ, Sharp IR, Moustafa AR, Leppard CW (2003) Normal fault growth, displacement localisation and the evolution of normal fault populations: the Hammam Faraun fault block, Suez rift. *Egypt J Struct Geol* 25(6):883–895
- Guo L, Riding R (1998) Hot-spring travertine facies and sequences, Late Pleistocene, Rapolano Terme, Italy. *Sedimentology* 45:163–180
- Hirani J (2014) *Diagenetic evaluation of fault/fracture related dolomitisation, Cretaceous-Eocene, Hammam Faraun Fault Block, Gulf of Suez*. Ph.D. thesis, University of Manchester, Manchester, United Kingdom, 295 p
- Hirani J, Bastesen E, Boyce A, Corlett H, Gawthorpe R, Hollis C, John CM, Robertson H, Rotevatn A, Whitaker F (2018a) Controls on the formation of stratabound dolostone bodies, Hammam Faraun Fault block, Gulf of Suez. *Sedimentology* 65(6):973–2002
- Hirani J, Bastesen E, Boyce A, Corlett H, Eker A, Gawthorpe R, Hollis C, Korneva I, Rotevatn A (2018b) Structural controls on non fabric-selective dolomitization within rift-related basin-bounding normal fault systems: Insights from the Hammam Faraun Fault Gulf of Suez Egypt. *Basin Res* 30(5):990–1014
- Hollis C, Bastesen E, Boyce A, Corlett H, Gawthorpe R, Hirani J, Rotevatn A, Whitaker F (2017) Fault-controlled dolomitization in a rift basin. *Geology* 45(3):219–222
- Issar A, Rosenthal E, Eckstein Y, Bogoch R (1971) Formation waters, hot springs and mineralization phenomena along the eastern shore of the Gulf of Suez. *Bull Int Assoc Sci Hydrol* 16:25–44
- Kerrick R (1986) Fluid infiltration into Fault Zones: chemical, isotopic and mechanical effects. *Pageoph* 124:225–268
- Kitano Y (1963) Geochemistry of calcareous deposits found in hot springs. *J Earth Sci Nagoya Univ* 11:68–100
- Korneva I, Bastesen E, Corlett H, Eker A, Hirani J, Hollis C, Gawthorpe RL, Rotevatn A, Taylor R (2018) The effects of dolomitization on petrophysical properties and fracture distribution within rift-related carbonates (Hammam Faraun Fault Block, Suez Rift, Egypt). *J Struct Geol* 108:108–120
- Kurlov MG (1928) Classification of mineral waters of Siberia. *Tomsk, USSR*
- Langelier WF, Ludwig HF (1942) Graphic method for indicating the mineral character of natural waters. *J Am Water Works Assoc* 34:335–352
- Lashin A (2013) A preliminary study on the potential of the geothermal resources around the Gulf of Suez. *Egypt Arab J Geosci* 6(8):2807–2828
- Magaritz M, Issar A (1973) Carbon and oxygen isotopes in epigenetic hydrothermal rocks from Hamam-El-Faraun. *Sinai Chem Geol* 12(2):137–146
- Mehmood M, Yaseen M, Khan EU, Khan JM (2018) Dolomite and dolomitization model - a short review. *Int J Hydro* 2(5):549–553
- Moeck IS (2014) Catalog of geothermal play types based on geologic controls. *Renew Sustain Energy Rev* 37:867–882
- Morgan P, Swanberg CA (1979) Heat flow and the geothermal potential of Egypt. *Pageoph* 117:213–225
- Morgan P, Boulos FK, Swanberg CA (1983) Regional geothermal exploration in Egypt. *Geophys Prospect* 31(2):361–376
- Morgan P, Boulos FK, Hennin SF, El-Sherif AA, El-Sayed AA, Basta NZ, Melek YS (1985) Heat flow in eastern Egypt: the thermal signature of a continental breakup. *J Geodyn* 4:107–131
- Moustafa AM (1976) Block faulting in the Gulf of Suez. In: *Proceedings of the 5th Egyptian General Petroleum Corporation Exploration Seminar, Cairo, Egypt*, 35 p
- Moustafa AR (2004) Geologic maps of the eastern side of the Suez rift (western Sinai Peninsula), Egypt. AAPG/Datapages. Inc. GIS

- Series (Geologic maps and cross-sections in digital format on CD and explanatory notes for the geologic maps)
- Moustafa AR, Abdeen MM (1992) Structural setting of the Hammam Faraun Block, eastern side of the Suez rift. *J Univ Kuwait (sci)* 19:291–310
- Moustafa AR, Khalil SM (2017) Control of extensional transfer zones on syntectonic and post-tectonic sedimentation: implications for hydrocarbon exploration. *J Geol Soc (London)* 174:318–335
- O'Neil JR, Barnes I (1971) C^{13} and O^{18} compositions in some freshwater carbonates associated with ultramafic rocks and serpentinites: western United States. *Geochim Cosmochim Acta* 35:687–697
- Patton TL, Moustafa AR, Nelson RA, Abdine SA (1994) Tectonic evolution and structural setting of the Suez Rift. In: Landon SM (ed) *Interior Rift Basins*. AAPG Mem, pp 9–55
- Pentecost A (2003) Cyanobacteria associated with hot spring travertines. *Can J Earth Sci* 40(11):1447–1457
- Rotevatn A, Bastesen E (2014) Fault linkage and damage zone architecture in tight carbonate rocks in the Suez Rift (Egypt): Implications for permeability structure along segmented normal faults. *Geol Soc London Spec Publ* 374:79–95
- Scholle PA, Ulmer-Scholle DS (2003) *A Color Guide to the Petrography of Carbonate Rocks: Grains, Textures, Porosity, Diagenesis*. AAPG Memoir 77, AAPG, Tulsa, Oklahoma
- Severin KP (2004) Energy dispersive spectrometry of common rock forming minerals. Kluwer Academic Publishers, p 225
- Shallaly NA, Beier C, Haase KM, Hammed MS (2013) Petrology and geochemistry of the Tertiary Suez rift volcanism, Sinai. *Egypt J Volcanol Geotherm Res* 267:119–137
- Sharp IR, Gawthorpe RL, Underhill JR, Gupta S (2000) Fault propagation folding in extensional settings: examples of structural style and synrift sedimentary response from the Suez rift, Sinai. *Egypt Geol Soc Am Bull* 112:1877–1899
- Shawky A (2020) Potentiality of geothermal energy resources of hammam Faraun area, south sinai governorate. Thesis registered at faculty of science, Cairo University, Egypt
- Sturchio NC, Arehart GB, Sultan M, Sano Y, AboKamar Y, Sayed M (1996) Composition and origin of thermal waters in the Gulf of Suez area. *Egypt Appl Geochem* 11:471–479
- Tucker ME (1991) Dolomitization, dedolomitization and silicification. In: *Sedimentary petrology: an introduction to the origin of sedimentary rocks*, 260 p
- Tucker ME, Wright VP (1990) Dolomites and Dolomitization Models. In: *Carbonate Sedimentology*, 482 p
- Warren J (2000) Dolomite: occurrence, evolution and economically important associations. *Earth Sci Rev* 52(1–3):1–81
- Weiszburg TG, Tóth E, Beran A (2004) Celadonite, the 10-Å green clay mineral of the manganese carbonate ore, Úrkút. *Hungary Acta Mineral-Petrogr* 45(1):65–80
- Wohletz K, Heiken G (1992) *Volcanology and geothermal energy*. University of California Press, p 432

Publisher's Note Springer Nature remains neutral with regard to jurisdictional claims in published maps and institutional affiliations.